

## Research article

# Nickel-doped willemite–liebenbergite composite pigments synthesis via a precipitation route involving silica hydrogel derived from serpentine minerals and its modification

Hayk Beglaryan, Anna Isahakyan<sup>\*</sup>, Anna Terzyan, Vardanush Stepanyan, Verzhine Sarkeziyan, Nshan Zulumyan

*Institute of General and Inorganic Chemistry of the National Academy of Sciences of the Republic of Armenia, Lane 2, Argutyan Street 10, Yerevan, 0051, Armenia*

## ARTICLE INFO

## Keywords:

Serpentine  
Silica hydrogel  
Precipitation approaches  
Nickel-doped willemite  
Liebenbergite  
Pigment

## ABSTRACT

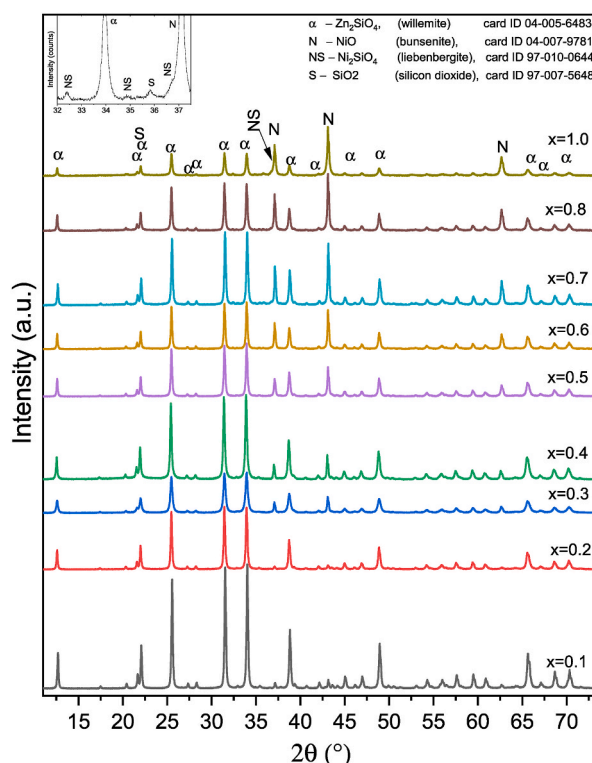
A simplified precipitation route involving silica hydrogel produced from serpentine-group minerals has been applied for pigment synthesis through the heat treatment of intermediates precipitated in the liquid phase, including  $\text{H}_2\text{O}$ ,  $\text{NaOH}$ ,  $\text{ZnCl}_2$ ,  $\text{NiCl}_2$ , and the silica hydrogel mentioned. Investigations have shown that this method is applicable for  $\text{Zn}_{2-x}\text{Ni}_x\text{SiO}_4$  compositions when  $x$  does not exceed 1.0 and pigments coloration in different blue or green hues is defined by certain proportions of phases crystallized in final products on heating from 900 up to 1200 °C, namely,  $\alpha\text{-Zn}_2\text{SiO}_4$  representing nickel-doped willemite, nickel oxide  $\text{NiO}$  and liebenbergite  $\text{Ni}_2\text{SiO}_4$ . The modification of the applied method has allowed performing the interaction between the reagents when  $x$  exceeds 1.0 thereby increasing the yield of  $\text{Ni}_2\text{SiO}_4$  phase in the products heated at 1200 °C from 70 up to about 90 ( $\pm 4$ ) % that actually remains unchangeable for  $x = 1.2 - 1.6$ . Liebenbergite increasing improves the color performance and stability of the synthesized green pigments in glaze.

## 1. Introduction

In comparison to cobalt-doped willemite  $\text{Zn}_{2-x}\text{Co}_x\text{SiO}_4$  ( $x \leq 0.5$ ) representing an excellent blue pigment with a low concentration of toxic cobalt, nickel-doped willemite system  $\text{Zn}_{2-x}\text{Ni}_x\text{SiO}_4$  is less studied [1–13]. A limited number of papers devoted to  $\text{Zn}_{2-x}\text{Ni}_x\text{SiO}_4$  synthesis and investigation report that either blue or green pigments can be produced via variation of nickel concentration introduced into initial systems due to different proportions of nickel-doped willemite  $\alpha\text{-Zn}_2\text{SiO}_4$  and nickel silicate  $\text{Ni}_2\text{SiO}_4$  formed in final products [1–6,11]. Nickel lower amount yields willemite phase formation, whereas nickel higher content promotes  $\text{Ni}_2\text{SiO}_4$  synthesis [3]. The latter called liebenbergite is classified as olivine green pigment [14]. It should be noted that liebenbergite is difficult to produce [15–19]. Conventionally, its production requires high temperature heat treatment (1200–1400 °C) lasting for hours regardless of silica  $\text{SiO}_2$  sources or routes whether it be ceramic, hydrothermal or geopolymerization methods [16,18,19]. Ni-doped willemite pigments synthesized via solid-state reaction method are also finally crystallized at high temperatures (about 1300 °C) maintained for several hours [7,11]. One of the ways of reducing this temperature up to 1000–1200 °C is either a mineralizer addition or replacement of commercial silica sources with industrial wastes such as rice husk ash or waste foundry sand [3–6]. An alternative option through

<sup>\*</sup> Corresponding author. Lane 2, Argutyan Street 10, Yerevan, 0051, Armenia.

E-mail addresses: [Isahakyananna@yahoo.com](mailto:Isahakyananna@yahoo.com), [hayk\\_b@ysu.am](mailto:hayk_b@ysu.am) (A. Isahakyan).



**Fig. 1.** XRPD patterns of the samples produced from the intermediates corresponding to  $\text{Zn}_{2-x}\text{Ni}_x\text{SiO}_4$  compositions with  $x$  ranging from 0.1 up to 1.0 via heat-treatment at 900 °C.

sol-gel processing suggests to use tetraethoxysilane (TEOS)  $\text{Si}(\text{OC}_2\text{H}_5)_4$  as a source of silica  $\text{SiO}_2$  for both  $\text{Zn}_{2-x}\text{Ni}_x\text{SiO}_4$  [1,2,8–10,12,13] and  $\text{Ni}_2\text{SiO}_4$  productions [15,17]. But this approach does not essentially simplify the procedures and conditions of their manufacturing either since it requires either durable intermediates preparation (12–48 h) [1,8,9] frequently combined with combustion or ultrasonic assistance [10,12,13,15] or long high-temperature calcination (5–6 h) [2,17]. It should be noted that one of the obligatory conditions for the mentioned methods related with TEOS is the involvement of additional reagents, particularly organic ones (ethanol  $\text{C}_2\text{H}_5\text{OH}$ , acetates, polyethylene glycol, diformyl hydrazine  $\text{C}_2\text{H}_4\text{N}_2\text{O}_2$ , tetraethylenepentamine, glucose) that complicates the whole procedure of  $\text{Zn}_{2-x}\text{Ni}_x\text{SiO}_4$  and  $\text{Ni}_2\text{SiO}_4$  syntheses and has relevant implications involving additional costs related with technological and ecological problems.

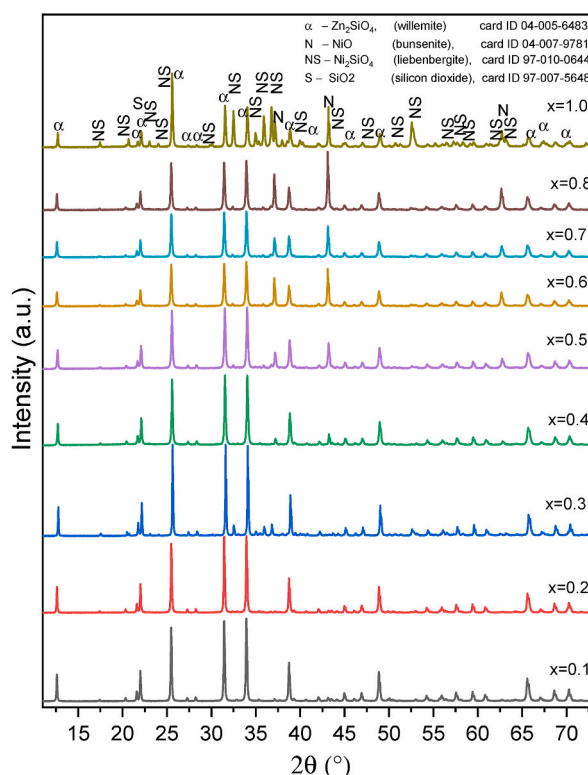
In this regard,  $\text{Zn}_{2-x}\text{Ni}_x\text{SiO}_4$  and  $\text{Ni}_2\text{SiO}_4$  compounds are expected to be produced at milder conditions via the precipitation route based on using silica hydrogel representing a co-product of serpentinites processing [20]. This expectation is encouraged by the promising results of the previous study devoted to  $\text{Zn}_{2-x}\text{Co}_x\text{SiO}_4$  production [21]. The findings obtained evidence that the involvement of this silica hydrogel in the precipitation stage does not only facilitate intermediates preparation and decrease the duration and temperatures of heat treatment for obtaining  $\text{Zn}_{2-x}\text{Co}_x\text{SiO}_4$  compounds but also allows avoiding the drawbacks related with TEOS and producing competitive blue pigments [21]. The advantage of this  $\text{SiO}_2$ -containing reagent over the rest of silicon dioxide sources is explained by the structural particularities of amorphous silica composing this hydrogel [22,23].

From the above reasoning, the precipitation method suggested was decided to apply for the introducing nickel ions in willemite structure. X-ray diffraction (XRD) study, Fourier transform infrared reflection (FTIR) spectroscopy, UV visible spectroscopy and Lab-color measurements as well as scanning electron microscopy (SEM) and energy dispersive spectroscopy (EDS) were involved for the investigation of both the intermediates precipitated and final products synthesized. A great attention was given to understanding factors responsible for colors variations and thermal stability of the final products and their performance in glaze.

## 2. Experimental

### 2.1. Chemicals

Nickel (II) chloride hexahydrate ( $\text{NiCl}_2 \cdot 6\text{H}_2\text{O}$ , puriss. p. a.,  $\geq 98\%$ , Sigma-Aldrich) was used as a dopant for nickel cations. Information about the other reagents, including a serpentine sample serving as a precursor for the silica hydrogel, and the production of the silica hydrogel is detailed in our earlier reports [21,24,25].



**Fig. 2.** XRPD patterns of the samples produced from the intermediates corresponding to  $\text{Zn}_{2-x}\text{Ni}_x\text{SiO}_4$  compositions with  $x$  ranging from 0.1 up to 1.0 via heat-treatment at 1000 °C.

## 2.2. Samples preparation

Samples corresponding to  $\text{Zn}_{2-x}\text{Ni}_x\text{SiO}_4$  compositions, where  $x$  is equal to 0.1, 0.2, 0.3, 0.4, 0.5, 0.6, 0.7, 0.8, 1.0 were synthesized following the precipitation procedure and heat treatment regime employed for the synthesis of Co-doped willemitite pigments [21].

The same precipitation procedure was applied to prepare suspensions from mixtures with  $\text{Zn}_{2-x}\text{Ni}_x\text{SiO}_4$  compositions, where  $x = 1.2, 1.4, 1.6, 1.8$ , and 2.0, which were then immediately heated to dryness in a boiling-water bath without filtration. The resulting mass was annealed at 900 °C and only then washed with distilled water. Five intermediates, washed after calcination at 900 °C, were subsequently subjected to a 60-min heat treatment at higher temperatures: 1000, 1100 and 1200 °C.

To accurately evaluate the coloring efficiency of the final samples, those synthesized from  $\text{Zn}_{1.9}\text{Ni}_{0.1}\text{SiO}_4$ ,  $\text{Zn}_{1.8}\text{Ni}_{0.2}\text{SiO}_4$ ,  $\text{Zn}_{1.7}\text{Ni}_{0.3}\text{SiO}_4$ ,  $\text{ZnNiSiO}_4$ ,  $\text{Zn}_{0.9}\text{Ni}_{1.1}\text{SiO}_4$ , and  $\text{Ni}_2\text{SiO}_4$  compositions were selected for testing in wall tile glaze. Six wall tile samples were coated with the pigment–glaze mixtures containing 10 wt% of the selected samples, using the glaze and procedures employed for Co-doped willemitite pigments [21]. The samples then underwent the heat-treatment at temperatures of 800, 900, 950, and 1000 °C, at a rate of 5 °C min<sup>−1</sup>, maintaining each target temperature for 60 min.

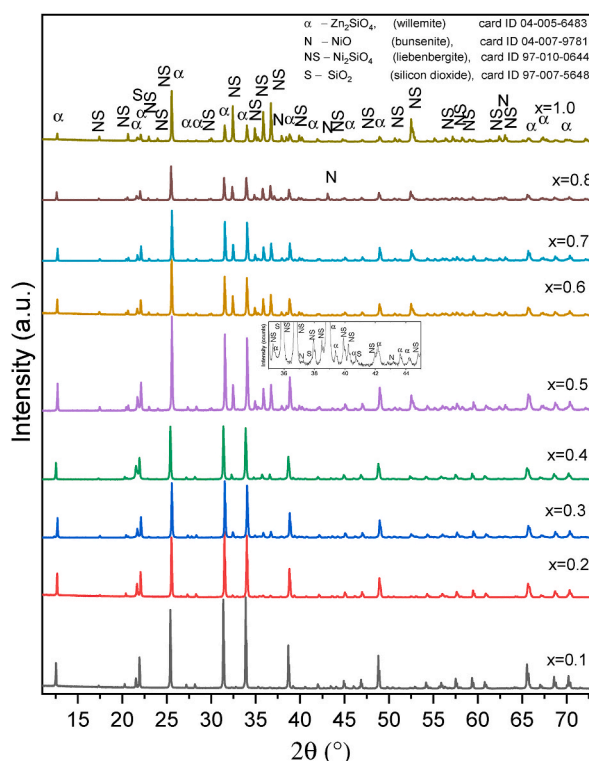
## 2.3. Characterization

A Smart Lab SE Rigaku multipurpose X-ray diffraction system (Japan), equipped with an XSPA-400 ER 2D detector, was employed to perform X-ray powder diffraction (XRPD) measurements. This enabled the determination of phase transformations in the intermediates during heating, phase composition of the final products, structure of the synthesized compounds, and particle size distribution. The analysis was conducted under the following conditions: Cu K $\alpha$  radiation, a power supply of 40 kV/50 mA, and an angular range of  $2\theta = 7^\circ$ – $75^\circ$  with a step size of 0.01° at room temperature in air.

Several of the final samples were subjected to FTIR analysis conducted on a Nicolet iS50 FT-IR spectrometer from Thermo Scientific, producing spectra in the 100–1300 cm<sup>−1</sup> range with a resolution of 2 cm<sup>−1</sup>.

Optical properties of the final samples and the glazed wall tile samples, in particular, absorption bands in the spectral range from 360 to 830 nm, were determined utilizing an Agilent Cary 60 UV–Vis spectrophotometer equipped with the reflector attachment. Halon served as a diffuse reflectance standard. The calculation of the chromatic parameters was performed based on the reflectance measurement data using CIE-L\*a\*b\* chromatic coordination system.

The surface morphology and elemental mapping images for several of the final samples were captured using a Prisma E SEM scanning electron microscope equipped with an energy dispersive spectrometer (EDS).



**Fig. 3.** XRPD patterns of the samples produced from the intermediates corresponding to  $\text{Zn}_{2-x}\text{Ni}_x\text{SiO}_4$  compositions with  $x$  ranging from 0.1 up to 1.0 via heat-treatment at 1100 °C.

### 3. Results and discussions

#### 3.1. XRD data

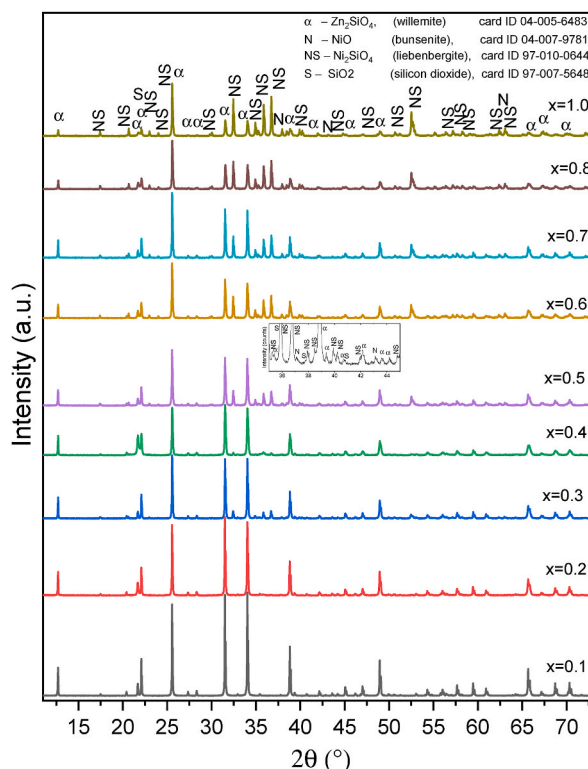
The XRPD patterns of  $\text{Zn}_{2-x}\text{Ni}_x\text{SiO}_4$  compositions where  $0.1 \leq x \leq 1.0$ , mainly show diffraction peaks matching with the standards of willemite with rhombohedral structure [26], nickel (II) oxide NiO, also known as bunsenite, and liebenbergite (Figs. 1–4).

At 900 °C the increasing nickel concentration in the initial system leads to a gradual increase in bunsenite phase co-existing with willemite phase. The latter remains dominant while the share of  $\text{Ni}_2\text{SiO}_4$  phase is very low (Fig. 1). These data point to the fact that, at 900 °C, a significant amount of NiO is formed, but only a negligible portion participates in the formation of  $\text{Ni}_2\text{SiO}_4$ . At 1000 °C NiO phase starts decreasing and this process is accompanied by liebenbergite phase increasing that is particularly noticeable for the samples with a higher content of nickel (Fig. 2). At 1100 °C, despite the increasing nickel amount in the system, NiO phase is barely detectable. Meanwhile, the share of liebenbergite phase, which was already observable for the samples with lower nickel concentrations, continues to increase gradually, resulting in the domination of liebenbergite phase compared to willemite phase (Fig. 3). Due to the crystallization of the amorphous silica unreacted the phase corresponding to the standard of silicon dioxide appears in the diffraction patterns at 1000 °C (Fig. 2) and exists on heating up to 1100 °C (Fig. 3) and higher (Fig. 4). Subsequent heating up to 1200 °C intensifies the phases registered at 1100 °C (Fig. 4). As a result, in the final products obtained at 1200 °C, with nickel increasing from  $x = 0.1$  up to  $x = 1.0$ , the share of liebenbergite phase grows from about 2 up to 70 %, while that of willemite phase drops from 98 up to 20 % (Fig. 5). At the same time the percentage of NiO and  $\text{SiO}_2$  phases is ranging from 0.5 up to 2.0 and from 2.0 up to 4.0, respectively (Fig. 5). According to the particle size distribution determined for willemite phase in the sample wherein it is about 98 % ( $x = 0.1$ ), the average particle size is estimated to be about 60 nm (Fig. 6).

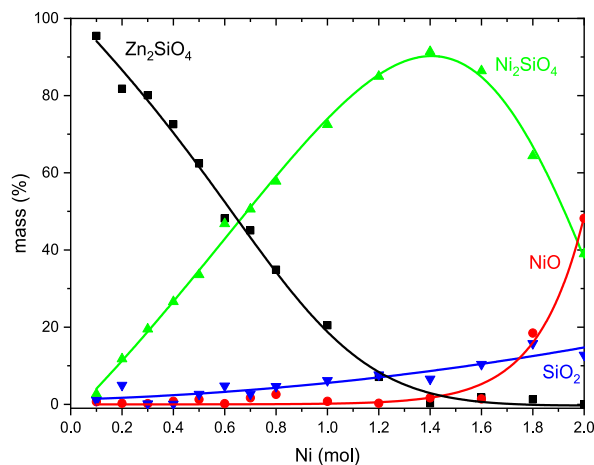
In order to perform the interaction between the reagents for  $\text{Zn}_{2-x}\text{Ni}_x\text{SiO}_4$  compositions where  $x$  exceeds 1.0, the precipitates prepared by the applied method were not immediately washed before calcination. This technique allowed using NaCl formed in the system during the stirring as a mineralizer on heating up to 900 °C.

Willemite and liebenbergite phases recorded in the diffraction patterns of  $\text{Zn}_{2-x}\text{Ni}_x\text{SiO}_4$  samples where  $1.2 \leq x \leq 2.0$  prepared via the novel approach to the precipitation method point to the interaction between the reagents for the above mentioned compositions (Figs. 7–10).

At 900 °C the increase of nickel amount in the initial mixture up to  $x = 1.2$  promotes the increasing of liebenbergite phase followed by the decreasing of willemite phase (Fig. 7). These processes continue up to  $x = 1.4$  and result in liebenbergite phase domination (Fig. 7). From  $x = 1.4$  up to  $x = 1.6$  no changes in phases are observable (Fig. 7). But when nickel content is increased up to  $x = 1.8$ , the abrupt increasing of NiO phase that is hardly traceable along with  $\text{SiO}_2$  phase for the compositions with a lower nickel content is



**Fig. 4.** XRPD patterns of the samples produced from the intermediates corresponding to  $\text{Zn}_{2-x}\text{Ni}_x\text{SiO}_4$  compositions with  $x$  ranging from 0.1 up to 1.0 via heat-treatment at 1200 °C.



**Fig. 5.** Curves presenting the tendencies of phase compositions change in the final products depending on nickel content.

accompanied by  $\text{Ni}_2\text{SiO}_4$  phase reduction (Fig. 7). Subsequent increase of nickel up to  $x = 2$  does not improve the situation (Fig. 7). Similar trends of the above mentioned phases towards increasing and decreasing are observed in the XRPD patterns of the same samples heated at 1000 (Figs. 8) and 1100 °C (Fig. 9). At 1200 °C, from  $x = 1.2$  up to  $x = 1.6$  willemite phase essentially reduces, and when  $x$  exceeds 1.6, despite NiO phase domination the portion of  $\text{Ni}_2\text{SiO}_4$  phase becomes noticeably increased, in comparison to the same samples heated at lower temperatures (Fig. 10). As can be seen, due to the modification implemented the portion of liebenbergite for  $x = 1.2$  at 1200 °C achieves about 90 ( $\pm 4$ ) % and remains practically unchangeable up to  $x = 1.6$  (Fig. 2). Liebenbergite synthesized has the orthorhombic structure and the average particle size equal to about 300 nm (Fig. 11).

These data indicate that the precipitation method suggested is applicable for  $\text{Zn}_{2-x}\text{Ni}_x\text{SiO}_4$  compositions where  $0.1 \leq x \leq 1.0$ , and since nickel ions concentration introduced into the willemite lattice is limited by  $\text{Zn}_{1.97}\text{Ni}_{0.03}\text{SiO}_4$  composition as follows from the

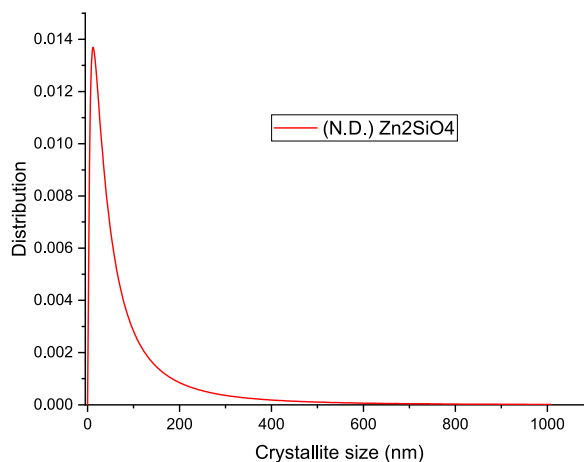


Fig. 6. Particle size distribution curve of willemite. (N.D.-the number distribution).

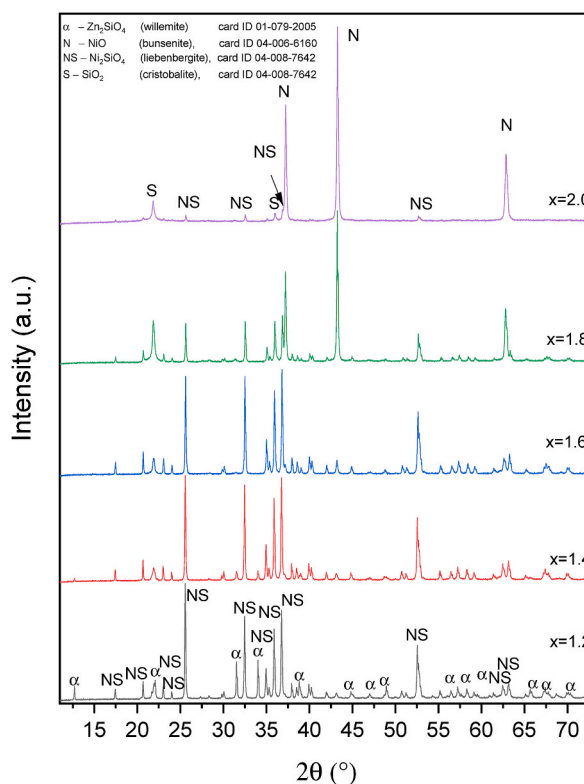
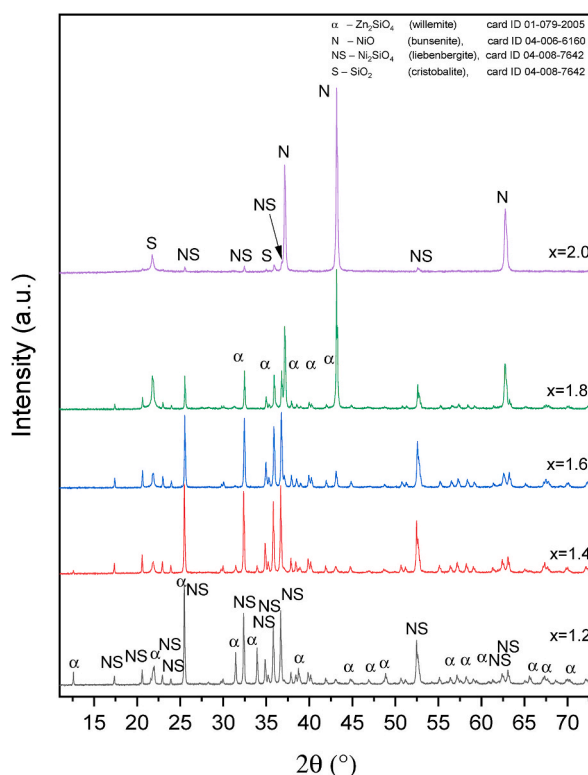


Fig. 7. XRPD patterns of the samples produced from the intermediates corresponding to  $\text{Zn}_{2-x}\text{Ni}_x\text{SiO}_4$  compositions with  $x$  ranging from 1.2 up to 2.0 after the heat-treatment at 900 °C.

previous report [11], nickel excess appeared in the diffraction patterns in the form of NiO on heating up to 1200 °C reacts with  $\text{SiO}_2$  remaining unreacted in the system yielding liebenbergite whose portion in the final product is about 70 %. The interaction between the reagents in the systems with  $x > 1.0$  does not occur as the reaction starts proceeding in the direction of generating nickel silicate whose formation requires special conditions including a mineralizer involvement. The modification of the applied method allowing to involve NaCl formed in situ as a mineralizer promotes liebenbergite formation when  $x$  exceeds 1.0 at such a low temperature as 900 °C. In addition, on heating up to 1200 °C the compositions with  $x$  ranging from 1.2 up to 1.6 are capable of yielding 90 ( $\pm 4$ ) % of liebenbergite in the final products.

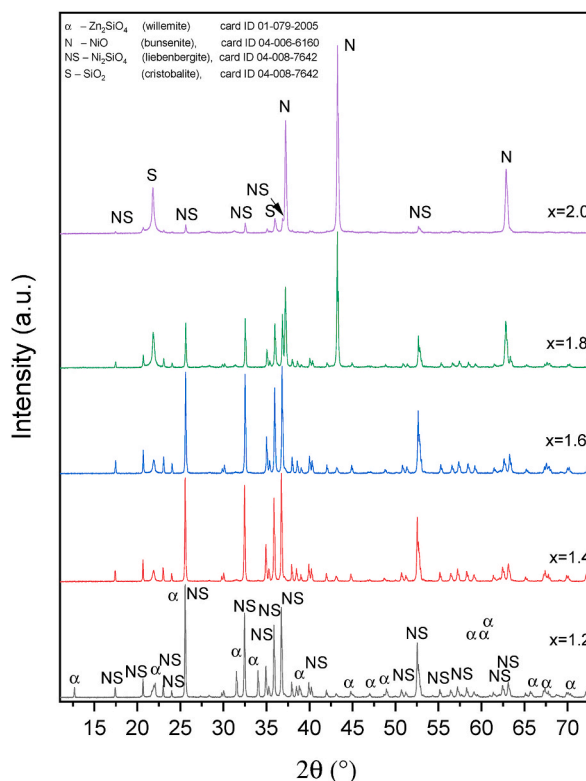


**Fig. 8.** XRPD patterns of the samples produced from the intermediates corresponding to  $\text{Zn}_{2-x}\text{Ni}_x\text{SiO}_4$  compositions with  $x$  ranging from 1.2 up to 2.0 after the heat-treatment at 1000 °C.

### 3.2. FTIR analysis

In the FT-IR spectra of  $\text{Zn}_{0.9}\text{Ni}_{0.1}\text{SiO}_4$ ,  $\text{Zn}_{1.5}\text{Ni}_{0.5}\text{SiO}_4$  and  $\text{ZnNiSiO}_4$  compositions heated at 1200 °C willemite phase is revealed by the appearance of vibration modes similar to pure willemite characteristic bands in the range of 860–1000 and 500–668  $\text{cm}^{-1}$ : at around 974, 928, 886, 861  $\text{cm}^{-1}$  and 460  $\text{cm}^{-1}$  caused by the stretching and banding vibrations of tetrahedron  $\text{SiO}_4$  anion isolated, respectively; 610 and 570  $\text{cm}^{-1}$  due to Zn-O vibrations of  $\text{ZnO}_4$  group (Figs. 12 and 13) [1,5,9,11–13]. If the spectral profile of  $\text{Zn}_{0.9}\text{Ni}_{0.1}\text{SiO}_4$  composition is almost identical to that of pure willemite synthesized by the precipitation method suggested (Fig. 12) [26],  $\text{Zn}_{1.5}\text{Ni}_{0.5}\text{SiO}_4$  and  $\text{ZnNiSiO}_4$  spectra exhibit four additional bands at around 825, 510 (shoulder), 484, which is moved to 475  $\text{cm}^{-1}$  in  $\text{ZnNiSiO}_4$  spectrum, and 325  $\text{cm}^{-1}$ , which are not seen in willemite spectrum (Fig. 13). Based on the fact that liebenbergite is detected by a number of peaks registered at around 978, 876 and 824  $\text{cm}^{-1}$ , and 583, 518 (shoulder) and 496  $\text{cm}^{-1}$  corresponding to stretching and bending vibrations of  $\text{SiO}_4$  anion, respectively [15,16], the appearance of the mentioned bands confirms  $\text{Ni}_2\text{SiO}_4$  phase formation along with willemite phase in  $\text{Zn}_{1.5}\text{Ni}_{0.5}\text{SiO}_4$  and  $\text{ZnNiSiO}_4$  samples. The rest of the peaks typical of liebenbergite is overlapped by willemite ones. Two weak bands traceable at above 1090 and 1200  $\text{cm}^{-1}$  in  $\text{Zn}_{0.9}\text{Ni}_{0.1}\text{SiO}_4$  and  $\text{Zn}_{1.5}\text{Ni}_{0.5}\text{SiO}_4$  spectra are attributed to cristobalite  $\text{SiO}_2$  crystallized from amorphous silica remaining unreacted in the system (Fig. 13) [27,28].

In the spectra of  $\text{Zn}_{0.8}\text{Ni}_{1.2}\text{SiO}_4$ ,  $\text{Zn}_{0.6}\text{Ni}_{1.4}\text{SiO}_4$  and  $\text{Zn}_{0.4}\text{Ni}_{1.6}\text{SiO}_4$  compositions where nickel is predominant, with the gradual increasing of nickel content up to  $x = 1.6$ , the bands at around 972, 825 and 325  $\text{cm}^{-1}$  identified with liebenbergite lattice become more distinct whereas the ones assigned to willemite mode disappear (Fig. 14). The spectra of  $\text{ZnNiSiO}_4$ ,  $\text{Zn}_{0.8}\text{Ni}_{1.2}\text{SiO}_4$ ,  $\text{Zn}_{0.6}\text{Ni}_{1.4}\text{SiO}_4$  and  $\text{Zn}_{0.4}\text{Ni}_{1.6}\text{SiO}_4$  display a couple of bands registered at around 957 and 852  $\text{cm}^{-1}$  which according to the literature data is not identified with liebenbergite lattice (Figs. 13 and 14). The appearance of these bands most probably implies the influence of zinc ions inserted into liebenbergite structure on the values of  $\text{SiO}_4$  group stretching vibrations. As for the band at around 876  $\text{cm}^{-1}$  serving for the identification of  $\text{Ni}_2\text{SiO}_4$ , it is most likely overlapped by the band at about 852  $\text{cm}^{-1}$  in these spectra and only becomes visible in the form of a weak band at 872  $\text{cm}^{-1}$  in the spectrum of  $\text{Ni}_2\text{SiO}_4$  composition when zinc is not involved into the reaction. In  $\text{Ni}_2\text{SiO}_4$  spectrum liebenbergite typical modes become much less intensive and two weak bands at 619 and 562  $\text{cm}^{-1}$  which are not registered in the rest of the spectra are demonstrated (Fig. 14). As the share of NiO in the products with compositions corresponding to  $\text{Zn}_{1-x}\text{Ni}_{1+x}\text{SiO}_4$  and  $\text{Ni}_2\text{SiO}_4$  is much higher than in the other samples (Fig. 6), they can probably be attributed to the bond-stretching vibrations of NiO [29–31]. The bands clearly seen at 1078 and 793  $\text{cm}^{-1}$  must be referred to O–Si–O asymmetric and Si–O–Si symmetric stretching vibrations of cristobalite, respectively [27,28] (Fig. 14).



**Fig. 9.** XRPD patterns of the samples produced from the intermediates corresponding to  $\text{Zn}_{2-x}\text{Ni}_x\text{SiO}_4$  compositions with  $x$  ranging from 1.2 up to 2.0 after the heat-treatment at 1100 °C.

### 3.3. Optical analysis

According to the data from literature sources a wide band with maxima at 534, 584 and 631 and another one with maximum at 777 nm recorded in the optical absorption spectra of  $\text{Zn}_{1.9}\text{Ni}_{0.1}\text{SiO}_4$  composition are typical of nickel-doped willemite ones [2,6,11–13] among which the first three of them correspond to  $3\text{T}_1(\text{F}) \rightarrow 3\text{T}_1(\text{P})$  d-d transition of  $\text{Ni}^{2+}$  ions in the tetrahedral environment and indicate the introduction of nickel into willemite lattice (Fig. 15) [2,13]. The temperature increasing up to 1200 °C promotes the growth of their absorbance (Fig. 15) pointing to a deep blue color consistent with the visual impression of the synthesized samples (Fig. 16).

At 1200 °C in  $\text{Zn}_{1.9}\text{Ni}_{0.1}\text{SiO}_4$  spectrum another band with the maximum at 422 nm is detected (Fig. 15). With the gradual increasing of nickel concentration starting from  $x = 0.3$  it starts becoming much more easily visualized along with nickel-doped willemite bands at 900 °C (Fig. 15). In addition, over 900 °C three more bands appear at 386, 475 and 710 nm (Fig. 15). Though the most noticeable ones recorded with the maxima at 422 and 710 nm result from the spin-allowed transitions of  $\text{Ni}^{2+}$  in octahedral coordination:  $^3\text{A}_2 \rightarrow ^3\text{T}_1(\text{P})$  and  $^3\text{A}_2 \rightarrow ^3\text{T}_1(\text{F})$ , respectively, they all indicate nickel inserted in olivine structure and can be therefore referred to  $\text{Ni}_2\text{SiO}_4$  responsible for green color (Fig. 16) [16,18]. Both the temperature and nickel concentration increasing promote their absorbance growth which starting from  $\text{Zn}_{1.6}\text{Ni}_{0.4}\text{SiO}_4$  composition is accompanied by nickel-doped willemite bands absorbance reduction (Fig. 15).

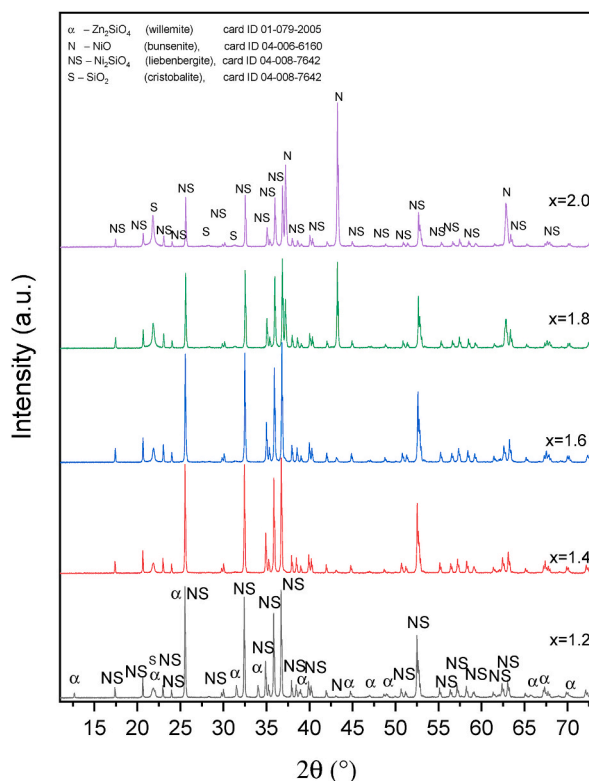
The band with the maximum at 380 nm seen at 900 °C in the spectra of almost all the samples refers to NiO remaining unreacted in the system (Fig. 15) [32,33]. Its absorbance decreases at higher temperatures due to the interaction between NiO and the amorphous  $\text{SiO}_2$  resulting in  $\text{Ni}_2\text{SiO}_4$  formation discovered by the four bands above mentioned (Fig. 15).

When nickel amount exceeds  $x = 1$ , the absorption curves mainly demonstrate  $\text{Ni}_2\text{SiO}_4$  typical absorption bands whose absorbance increases with the temperature rise (Fig. 17). This trend continues until nickel is increased up to  $x = 1.6$  including (Fig. 17) In the spectra of the samples where  $x \geq 1.8$  the increasing absorbance of NiO band recorded along with the decreasing absorbance of  $\text{Ni}_2\text{SiO}_4$  bands confirms the negative influence of subsequent increase of nickel concentration on  $\text{Ni}_2\text{SiO}_4$  formation (Fig. 17).

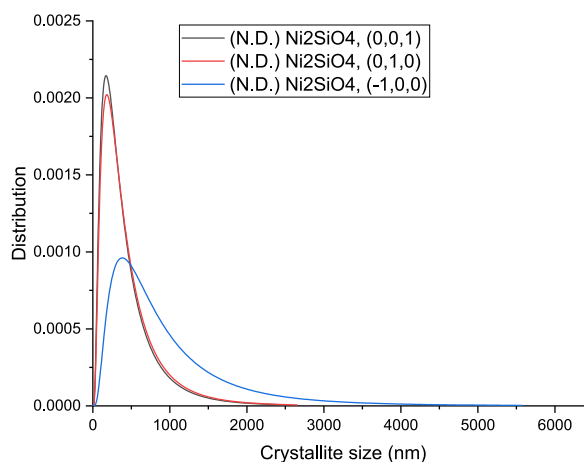
As can be seen, changes in the shape and the position of bands in the spectra of all the samples are in accordance with the phases crystallized in different proportions in each of the compositions depending on nickel concentration and temperature.

#### 3.3.1. Color

Different hues of blue and green are observable in the final products synthesized from initial mixtures with  $\text{Zn}_{2-x}\text{Ni}_x\text{SiO}_4$  compositions, where  $x$  ranges from 0.1 to 1.0, after heating from 900 to 1200 °C (Fig. 16). When  $x$  exceeds 1.0, only green shades are



**Fig. 10.** XRPD patterns of the samples produced from the intermediates corresponding to  $\text{Zn}_{2-x}\text{Ni}_x\text{SiO}_4$  compositions with  $x$  ranging from 1.2 up to 2.0 after the heat-treatment at 1200 °C.



**Fig. 11.** Particle size distribution curves of liebenbergite.

obtained (Fig. 18).

The products with nickel content corresponding to  $0.1 \leq x \leq 0.4$  display different hues of blue color depending on nickel concentration and heat-treatment temperature (Fig. 16). The increase of  $b^*$  (blue component) in negative and the decrease of positive  $L^*$  (lightness) parameters are observed with the temperature rise (Table 1). Both the more negative  $b^*$  and the lower positive  $L$  values achieved at 1200 °C ( $L^*/b^* = 53.87/-45.54$ ,  $33.61/-23.61$ ,  $52.93/-20.24$ ,  $55.89/-33.29$  for  $\text{Zn}_{0.9}\text{Ni}_{0.1}\text{SiO}_4$ ,  $\text{Zn}_{0.8}\text{Ni}_{0.2}\text{SiO}_4$ ,  $\text{Zn}_{0.7}\text{Ni}_{0.3}\text{SiO}_4$ ,  $\text{Zn}_{0.6}\text{Ni}_{0.4}\text{SiO}_4$  compositions, respectively) point to the positive effect of temperature increase on blue color saturation (Table 1). At the same time, increased nickel concentration does not enhance blue color intensity, as shown by the most negative  $b^*$  value (-45.54) recorded at 1200 °C for the  $\text{Zn}_{0.9}\text{Ni}_{0.1}\text{SiO}_4$  composition compared to the other samples (Table 1). At the same time, the increase of nickel concentration does not promote the improvement of blue color saturation as indicated by the most negative  $b^*$  value

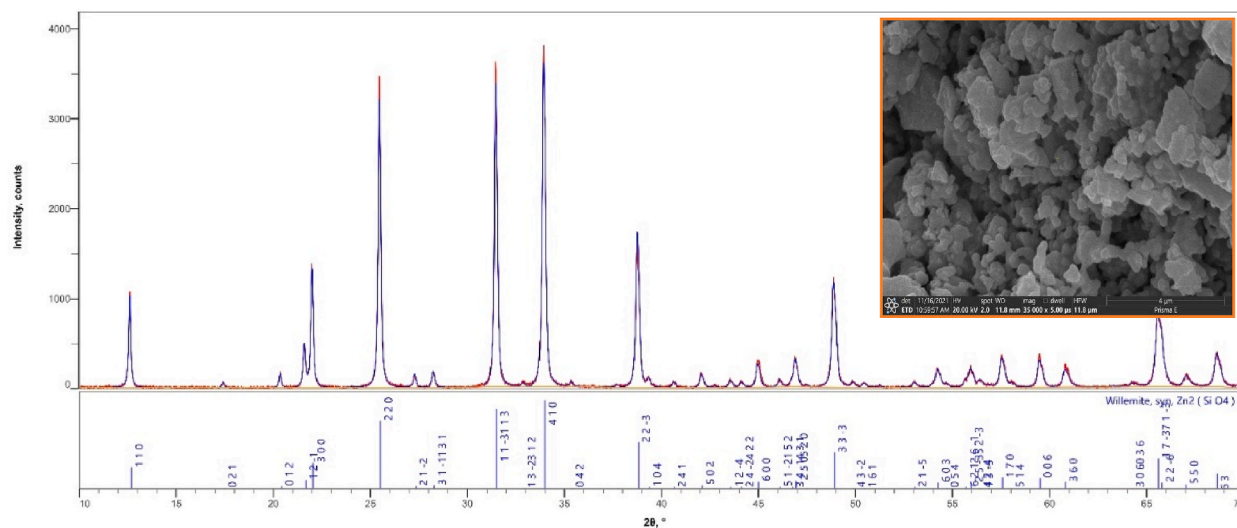


Fig. 12. The XRPD pattern and the SEM image of the pure willemite sample synthesized by the precipitation route suggested.

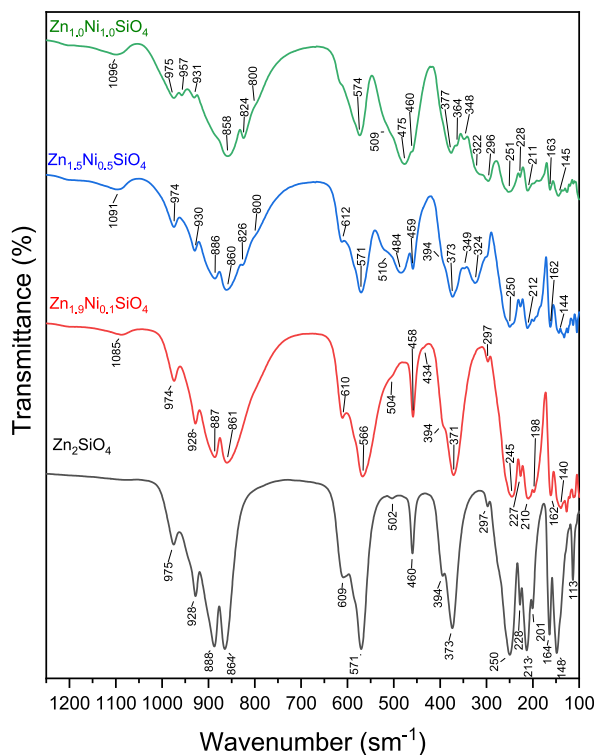
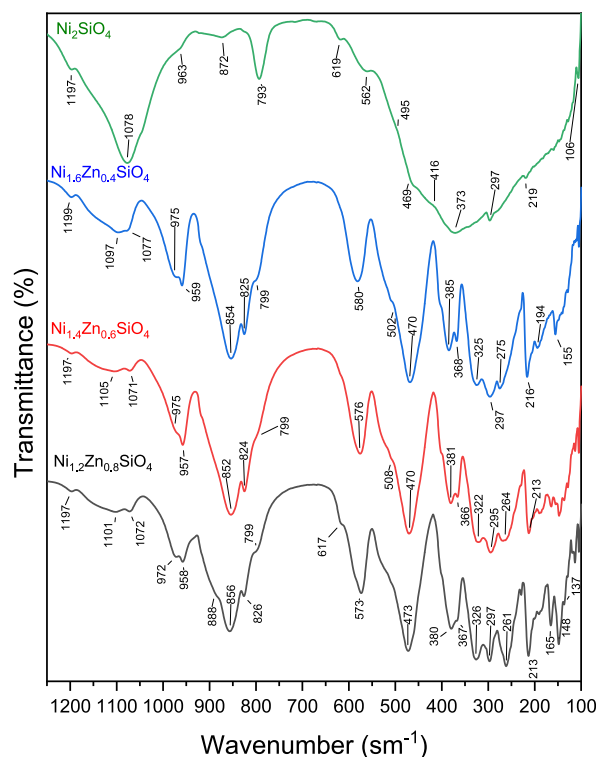


Fig. 13. FTIR spectra of the samples corresponding to  $\text{Zn}_{2-x}\text{Ni}_x\text{SiO}_4$  compositions where  $0.1 \leq x \leq 1.0$  prepared by the precipitation method.

(-45.54) recorded at 1200 °C for  $\text{Zn}_{0.9}\text{Ni}_{0.1}\text{SiO}_4$  composition compared to the other samples (Table 1).

The decreasing of blue color intensity traceable with the increasing of nickel content from  $x = 0.1$  up to  $x = 0.4$  (Table 1) is conditioned by the gradual growth of  $\text{Ni}_2\text{SiO}_4$  phase share achieving about 30 % in the final sample whereas the portion of willemite phase implying Ni-doped willemite responsible for blue hue saturation is reduced from 98 up to about 70 % as is evident from the relevant XRPD patterns (Figs. 1–5).

The subsequent increase of nickel content in the initial mixture ( $0.5 \leq x \leq 1.0$ ) generates green colorations of the products (Fig. 16). This change in color is perfectly adequate to alternations in the color coordinates (Table 1). From  $x = 0.4$  to  $x = 0.5$  at 1100 °C the abrupt increase of the parameters of  $a^*$  in negative (-15.38) belonging to green component and  $b^*$  in positive (6.43) corresponding to



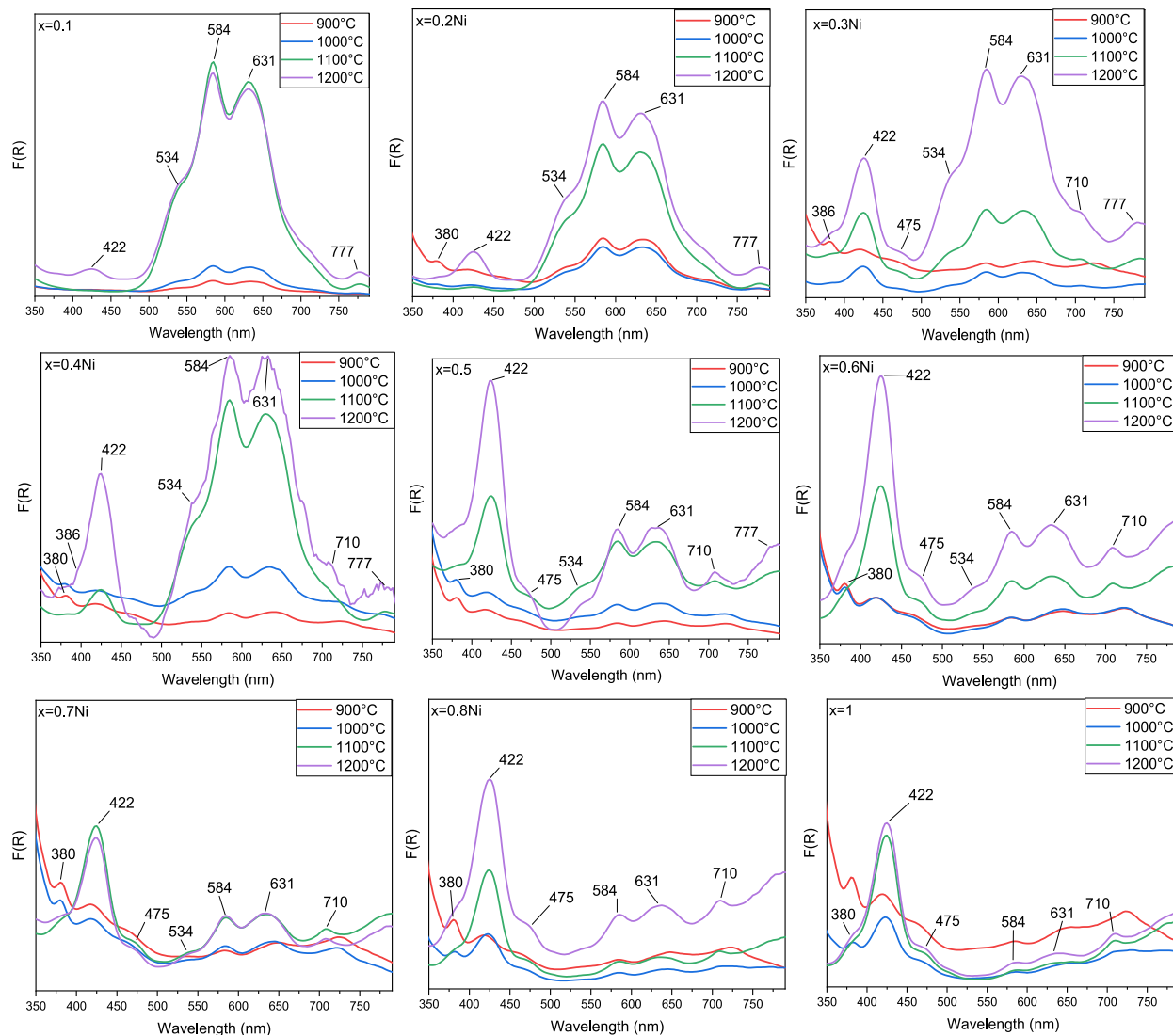
**Fig. 14.** FTIR spectra of the samples corresponding to  $\text{Zn}_{2-x}\text{Ni}_x\text{SiO}_4$  compositions where  $1.2 \leq x \leq 2.0$  prepared by the modified approach to this method.

yellow component are registered. The rest of the samples also demonstrate the trend toward increasing the share of green component over 1000 °C. Over 900 °C the further gradual increasing of nickel up to  $x = 0.7$  does not essentially influence on  $b^*$  parameter ranging from 5.39 up to 7.92. But when nickel content is increased up to  $x = 0.8$ ,  $b^*$  value starts abruptly increasing from 6.69 up to 11.54 at 1100 °C and achieves 13.31 at 1200 °C. For  $x = 1.0$  at 1000 and 1100 °C the abrupt increase of yellow component from 8.41 up 15.68 and from 15.68 up to 21.56 are also observable, respectively. A minor change in the values of both  $a^*$  (from -16.30 up to -17.46) and  $b^*$  (from 21.56 up to 20.53), observed as the temperature rises from 1100 to 1200 °C for  $x = 1.0$ , reveals the positive influence of increased nickel content on color stability, which can be explained by the increasing amount of  $\text{Ni}_2\text{SiO}_4$  formed in the system.

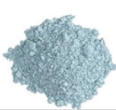
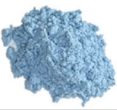



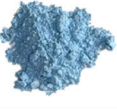



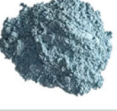
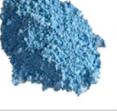
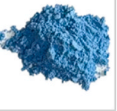
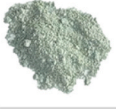
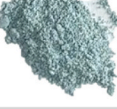
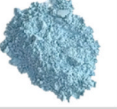

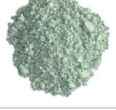
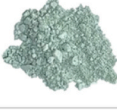




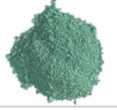





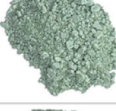
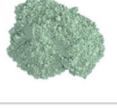
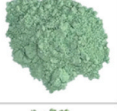





Further nickel increase ( $1.2 \leq x \leq 2.0$ ), which became realizable due to the implementation of the modified approach to the precipitation method, continues the trends of  $L^*$  and  $b^*$ , and  $a^*$  parameters towards increasing in positive and negative, respectively, on heating (Table 2). As a result, both the higher positive  $L^*$  and  $b^*$  and the higher negative  $a^*$  values are estimated from  $x = 1.2$  up to  $x = 1.6$  at 1000 °C and higher in comparison to the samples with the lower doping level ( $0.1 \leq x \leq 1.0$ ) (Table 2). In contrast with the samples from  $x = 1.2$  up to  $x = 1.6$ , from  $x = 1.8$  and  $x = 2.0$  much lower values of positive  $L^*$  and  $b^*$  and negative  $a^*$  are measured at the same temperatures (Table 2). A minor difference between each of  $L^*$ ,  $a^*$  and  $b^*$  parameters are traceable from  $x = 1.4$  and  $x = 1.6$  on heating from 1000 up to 1200 °C:  $L^*/a^*/b^* = 78.22/-17.34/36.90$ ;  $L^*/a^*/b^* = 78.41/-19.27/41.65$ ;  $L^*/a^*/b^* = 73.87/-20.91/43.34$  for  $x = 1.4$  and  $L^*/a^*/b^* = 80.49/-16.81/37.62$ ;  $L^*/a^*/b^* = 79.83/-18.89/41.07$ ;  $L^*/a^*/b^* = 78.61/-19.86/41.60$  for  $x = 1.6$  at 1000, 1100 and 1200 °C, respectively (Table 2). These data indicate that these samples practically show the similar hues of yellowish green color distinguished by thermal stability on heating.

As follows from the color evolution and measurements, pure green color is achieved at 1200 °C in  $\text{Zn}_{1.5}\text{Ni}_{0.5}\text{SiO}_4$  composition exhibiting the higher negative green component ( $a^* = -15.01$ ) and the lowest yellow one ( $b^* = 0.49$ ) (Table 1). Relatively low proportions of yellow component measured for  $x = 0.5$  at 1100 °C and for  $0.6 \leq x \leq 0.8$  over 900 °C (Table 1) account for dark green hues seen in the relevant samples (Fig. 16). The higher share of yellow component estimated for  $x = 1.0$  at 1100 °C results in the transformation of this shade into yellowish green one which remains thermally stable when heated up to 1200 °C (Table 1) (Fig. 16). With the subsequent nickel increase yellowish green hue starts changing into lighter one stable from 1000 up to 1200 °C for  $x = 1.4$ –1.6 (Fig. 18). This type of tints is achieved due to relatively stable green component  $a^*$  ranging from -16.81 to -20.91 supported by a noticeable increase in both yellow component  $b^*$  and lightness  $L^*$  falling in the range of 36.90–43.34 and 73.87–80.49, respectively (Table 2). When  $x$  exceeds 1.6, this hue becomes darker again (Fig. 18) due to the reduced portions of yellow component  $b^*$  and lightness  $L^*$  (Table 2).

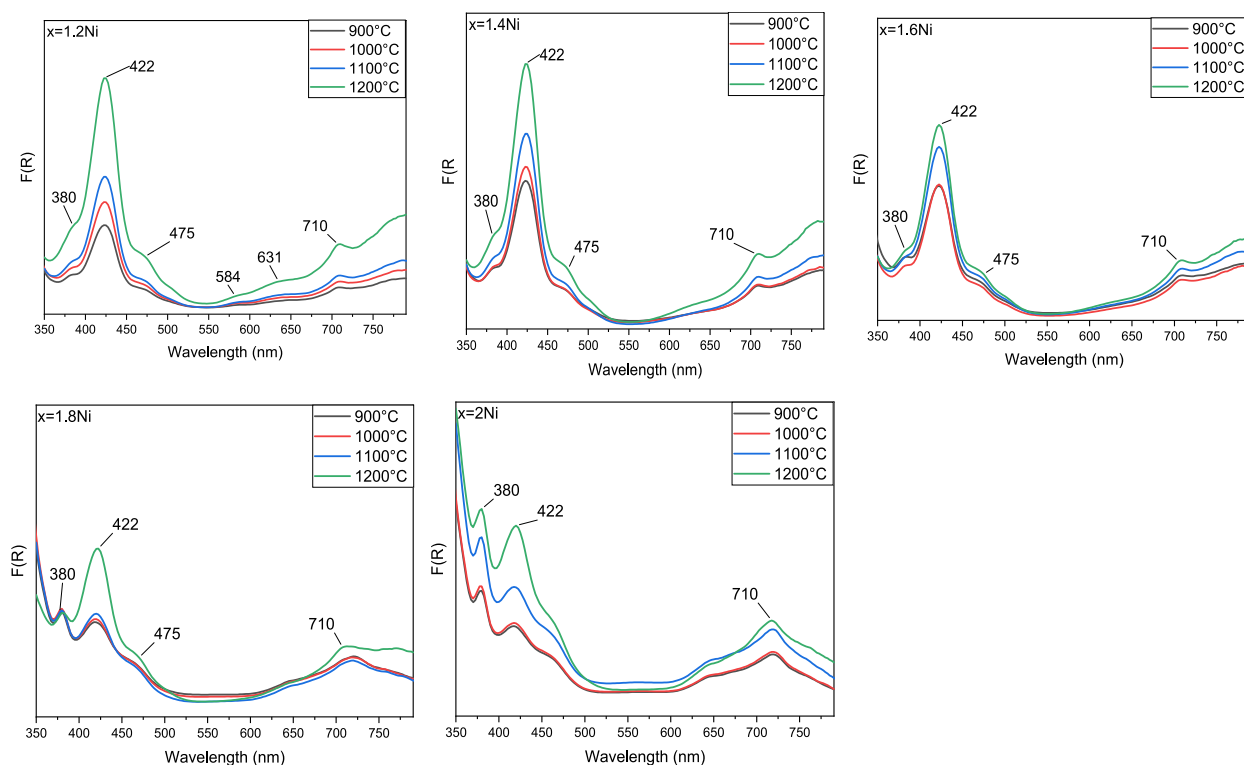
The comparison of the phases discovered in the XRPD patterns (Fig. 5) with the color data obtained for the relevant samples (Tables 1 and 2) allows to conclude that the shade and the stability of green color obtained in  $\text{Zn}_{2-x}\text{Ni}_x\text{SiO}_4$  systems where  $0.5 \leq x \leq 2.0$  depends on the portion of  $\text{Ni}_2\text{SiO}_4$  formed along with willemite and NiO phases in systems. A wide spectrum of yellowish-green tints



**Fig. 15.** Absorbance spectra of the samples precipitated from  $\text{Zn}_{2-x}\text{Ni}_x\text{SiO}_4$  compositions where  $0.1 \leq x \leq 1.0$  and then heated at different temperatures. Ni-doped willemite-related bands: at 534, 584, 631, 777 nm;  $\text{Ni}_2\text{SiO}_4$ -related bands: at 386, 422, 475, 710 nm; NiO-related band: at 380 nm.

$x \backslash t^{\circ}\text{C}$	900	1000	1100	1200
0.1				
0.2				
0.3				
0.4				
0.5				
0.6				
0.7				
0.8				
1.				

**Fig. 16.** The digital images of the samples produced from  $\text{Zn}_{2-x}\text{Ni}_x\text{SiO}_4$  compositions with  $x$  ranging from 0.1 up to 1.0 on heating from 900 up to 1200 °C.



**Fig. 17.** Absorbance spectra of the samples produced from  $\text{Zn}_{2-x}\text{Ni}_x\text{SiO}_4$  compositions where  $1.2 \leq x \leq 2.0$  by the modified approach to the precipitation method and then heated at different temperatures. Ni-doped willemite-related bands: at 584 and 631 nm; Ni<sub>2</sub>SiO<sub>4</sub>-related bands: at 422, 475 and 710 nm; NiO-related band: at 380 nm.



**Fig. 18.** The digital images of the samples produced from  $Zn_{2-x}Ni_xSiO_4$  compositions with x ranging from 1.2 up to 2.0 by the modified approach to the precipitation method and then heated at different temperatures from 900 up to 1200 °C.

**Table 1**

CIE-Lab parameters of  $\text{Zn}_{2-x}\text{Ni}_x\text{SiO}_4$  samples synthesized from the corresponding intermediates prepared by the precipitated method via heat treatment at different temperatures.

x		900 °C	1000 °C	1100 °C	1200 °C
0.1	L*	78.65	74.59	41.82	53.87
	a*	-3.59	-3.75	-0.43	7.46
	b*	-5.25	-13.06	-26.01	-45.55
0.2	L*	64.87	71.22	62.33	33.61
	a*	-7.16	-5.39	-4.19	1.91
	b*	-7.96	-17.47	-30.15	-23.61
0.3	L*	60.26	67.66	67.60	52.94
	a*	-7.93	-5.81	-5.89	-4.47
	b*	-8.06	-10.18	-18.85	-20.24
0.4	L*	77.63	76.00	77.78	55.89
	a*	-6.68	-4.20	-8.45	-3.25
	b*	4.83	-10.60	-9.99	-33.29
0.5	L*	73.02	57.36	68.12	63.39
	a*	-7.46	-6.75	-15.38	-15.01
	b*	6.32	3.05	6.43	0.49
0.6	L*	77.56	79.45	75.79	72.72
	a*	-9.68	-13.05	-12.19	-17.11
	b*	7.06	7.10	5.87	7.92
0.7	L*	67.82	73.66	68.14	63.27
	a*	-7.31	-8.87	-16.00	-15.77
	b*	12.19	7.12	7.78	5.39
0.8	L*	66.92	70.56	81.93	74.23
	a*	-2.87	-7.78	-11.35	-14.13
	b*	3.57	6.69	11.54	13.31
1	L*	65.20	83.80	73.55	73.41
	a*	-7.34	-13.30	-16.30	-17.47
	b*	8.41	15.68	21.56	20.53

obtained is the consequent of liebenbergite formed in different amount. It has become apparent the more liebenbergite is synthesized, the lighter yellowish green hue is generated. As a result, the amount of liebenbergite obtained in the system where  $x = 1$  is sufficient for providing yellowish-green coloration stable from 1100 up to 1200 °C. The highest portion of liebenbergite provided by  $x = 1.4$ – $1.6$  guarantees the stability of lighter yellowish-green hues from 1000 up to 1200 °C. Darker green shades apparent in the products wherein  $x$  exceeds 1.6 is caused by liebenbergite lower concentration along with the increasing amount of NiO.

### 3.4. SEM & EDX

The SEM image of  $\text{Zn}_{1.9}\text{Ni}_{0.1}\text{SiO}_4$  sample exhibits a relatively homogeneous well-defined spherical shaped morphology (Fig. 19a) similar to the microstructure of pure willemite (Fig. 12). This fact indicates that low concentrations of  $\text{Ni}^{2+}$  ions have no essential influence on willemite morphology. In the micrograph of  $\text{Zn}_{1.5}\text{Ni}_{0.5}\text{SiO}_4$  sample this homogeneity is destroyed by the appearance of particles with more or less regular shapes quite different from willemite ones (Fig. 19b). As observed for  $\text{ZnNiSiO}_4$ , the number of this type of grains co-existing with willemite particles increases with increasing of nickel concentration (Fig. 19c). The formation of a relatively homogeneous microstructure composed of well-formed uniform crystals presenting prismatic shape is seen in  $\text{Zn}_{0.4}\text{Ni}_{1.6}\text{SiO}_4$  image (Fig. 19d). The comparison of the images with the crystalline phases evolution in the relevant XRPD patterns points to the fact that these crystals belong to  $\text{Ni}_2\text{SiO}_4$  (Fig. 5).  $\text{Ni}_2\text{SiO}_4$  image presents crystals with relatively large dimensions (Fig. 19e).

Besides Zn, Ni, O, Si elements which are the main constituents of the final products, the EDS analysis of the samples above mentioned identify C, Al and Na (Fig. 20a–d). Carbon must be one of the component of  $\text{CO}_2$  absorbed from the air and often discovered in EDS spectra. Al atoms appear due to aluminum conductive coating on the surface of the samples. Sodium is likely present due to residual sodium silicate that didn't react, as well as adsorbed Na ions within the system. The elemental compositions and concentrations observed in the products align with the initial molar ratios of the reactants.

**Table 2**

CIE-Lab parameters of  $\text{Zn}_{2-x}\text{Ni}_x\text{SiO}_4$  samples synthesized from the corresponding intermediates prepared by the modified approach to the precipitated method via heat treatment at different temperatures.

x		900 °C	1000 °C	1100 °C	1200 °C
1.2	L*	76.90	76.35	75.75	67.63
	a*	-14.23	-17.02	-19.41	-20.95
	b*	27.18	28.93	31.83	34.31
1.4	L*	75.06	78.22	78.41	73.87
	a*	-14.41	-17.34	-19.27	-20.91
	b*	33.67	36.90	41.65	43.34
1.6	L*	76.35	80.49	79.83	78.61
	a*	-14.90	-16.81	-18.89	-19.86
	b*	34.01	37.62	41.07	41.60
1.8	L*	63.93	68.04	70.91	70.39
	a*	-9.98	-11.21	-13.90	-15.61
	b*	19.80	22.31	26.54	31.44
2	L*	62.98	65.56	65.59	65.78
	a*	-10.77	-10.68	-11.97	-14.12
	b*	19.29	19.60	21.59	29.31

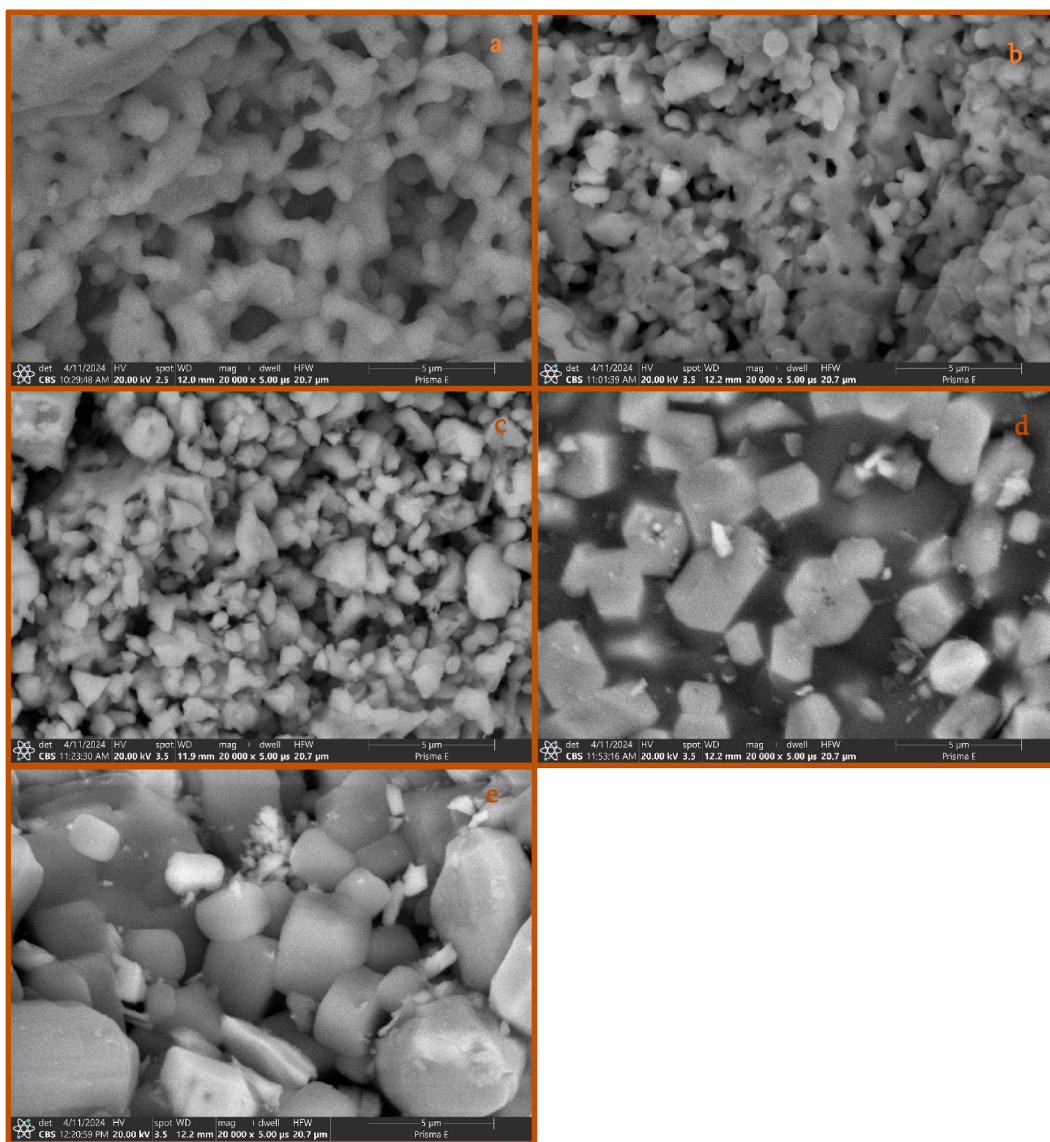
### 3.5. Color performance

In order to compare the behavior of the samples applied in the glaze depending on temperature, color measurements of the wall tile samples prepared at different temperatures from the ceramic glaze and 10 wt% of the pigments corresponding to  $\text{Zn}_{2-x}\text{Ni}_x\text{SiO}_4$  compositions with  $x = 0.1, 0.5, 0.7, 1.0, 1.6$ , and  $2.0$  were carried out. The values of  $L^*a^*b^*$  parameters for each of the wall tile samples (Table 3) are different from those corresponding to its pigment and this difference becomes more significant on heating over  $800^\circ\text{C}$  (Tables 1 and 2). The more noticeable changes occur for the samples with  $x \leq 1.0$ :  $a^*$  green components decrease three and more times from about  $-15$  –  $-16$  measured for the pigments (Table 1) up to about  $-1$  –  $-8$  for the pigments applied (Table 3), for  $x \leq 0.7$   $b^*$  yellow components drastically increase from  $0.5$  –  $8$  (Table 1) up to  $14.47$  –  $19.57$  (Table 3), whereas for  $x = 1$  the difference between  $b^*$  values reduces (Tables 1 and 3), as for  $b^*$  blue component that achieves the higher negative value equal to  $-45.55$  in the sample with  $x = 0.1$  (Table 1) thus providing the deepest blue hue, its value twice increases up to  $-24.14$  and continues growing up to  $14.83$  on heating when being tested into the glaze (Table 3). Though the difference between each of  $a^*$  and  $b^*$  values continues reducing with the increase of nickel content, the tendency of  $-a^*$  green component to diminish is still traceable for the samples with  $x = 1.6$  and  $x = 2$  after the application, whereas  $b^*$  yellow component starts decreasing (Tables 2 and 3). These observations confirm that the synthesized compounds partly decomposed in the glaze due to the decomposition of Ni-doped willemite which is not stable in glaze thereby imparting light brown color to the wall tile samples glazed provided that the pigments largely composed of Ni-doped willemite phase are used [3,34].

The behavior of the pigments applied in the glaze also differs from one composition to another on heating (Table 3). From  $800$  up to  $950^\circ\text{C}$  the increasing of nickel up to  $x = 1.6$  is accompanied by the increase of lightness  $L^*$  from  $56$  –  $72$  up to about  $85$  –  $87$  which at  $1000^\circ\text{C}$  reduces up to about  $75$  –  $77$  for  $0.5 \leq x \leq 1.0$ , remains unchangeable ( $84$  –  $85$ ) for  $x = 1.6$  (Table 3). For  $x = 2.0$  it increases from  $60$  up to  $72$  on heating from  $800$  up to  $900^\circ\text{C}$ , then remains unchangeable up to  $950^\circ\text{C}$  and achieves  $78.71$  at  $1000^\circ\text{C}$  (Table 3). Concerning  $-a^*$  and  $+b^*$  chromatic parameters responsible for yellowish-green shade, with the increase of nickel concentration up to  $x = 1.6$  they increase and reach about  $-11.5$  and  $26$ , respectively, but when nickel increases up to  $x = 2.0$ , these values reduce up to  $-9$  and  $20$  –  $23$ , respectively (Table 3). The most negative  $-a$  value ( $-11.5$ ) and the highest yellow component ( $26$ ) which are not influenced of temperature are observed for the wall tile sample prepared from the glaze containing the pigment with  $x = 1.6$  (Table 3).

The effect of the glaze medium on the stability of the compounds previously crystallized in the synthesized pigments has been also shown via the UV–Vis spectra recorded for the relevant samples (Fig. 21). At  $800^\circ\text{C}$  the absorption curves of all the glazed samples are generally close to the ones of the adequate pigments, in other words, they demonstrate the similar profiles and bands positions revealing Ni-doped willemite (at  $534, 584$  and  $631$  nm), liebenbergite (at  $422, 475$  and  $710$  nm) as well as bunsenite (at  $380$  nm) presence in the corresponding systems (Fig. 21). On heating over  $800^\circ\text{C}$  Ni-doped willemite-related bands disappear (Fig. 21). As for liebenbergite and bunsenite absorption peaks, despite a decrease in their intensities displayed at  $900^\circ\text{C}$  subsequent heating does not already significantly affect the degree of their absorbance (Fig. 21).

These data indicate that the gradual increasing of liebenbergite portion in the final products improves both the color intensity and color stability of the synthesized green pigments resulting in the production of such a green pigment corresponding to  $x = 1.2$  –  $1.6$  that due to the highest concentration of liebenbergite demonstrates the most excellent color performance and higher stability in the glaze.

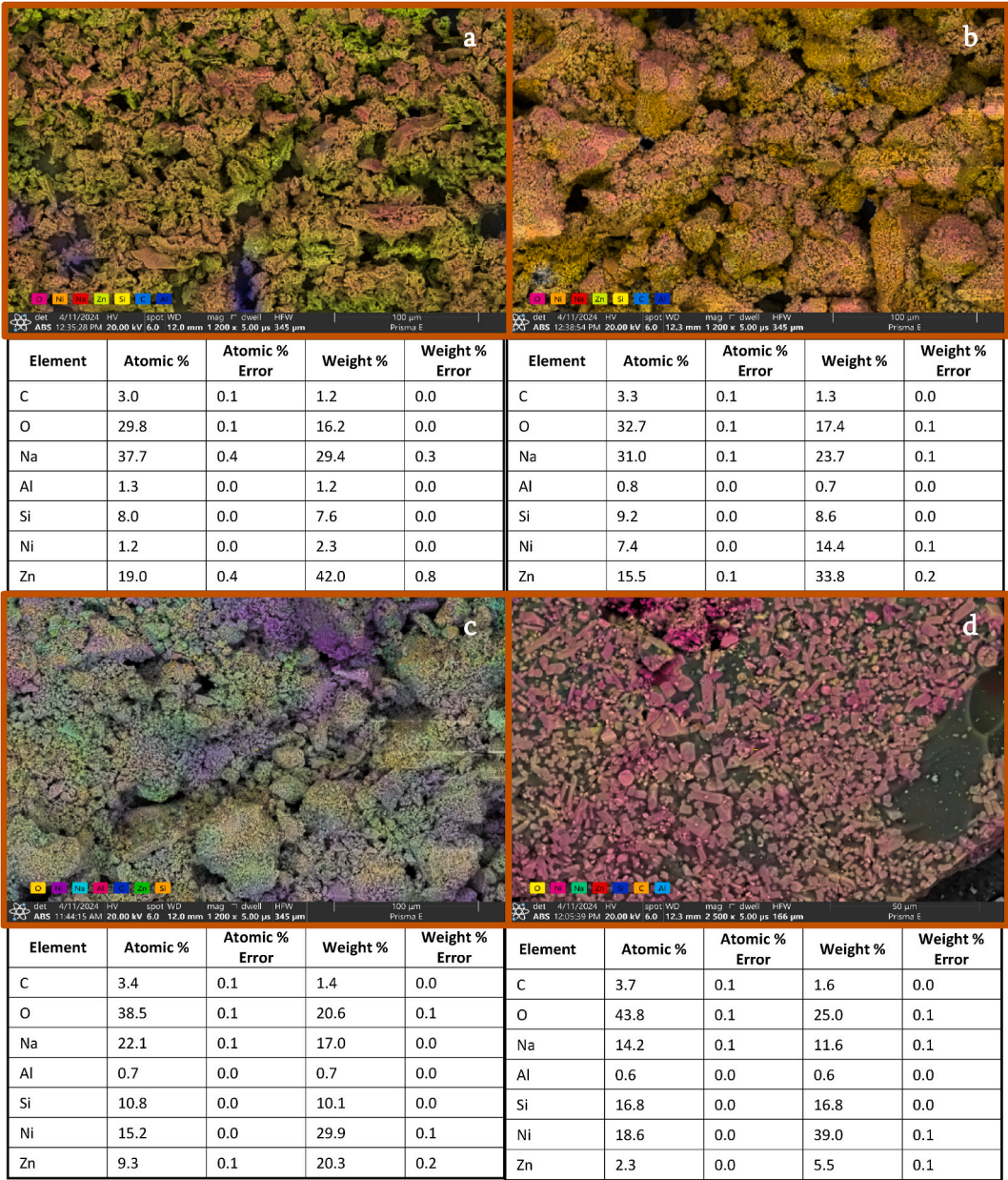


**Fig. 19.** SEM images of the samples corresponding to  $\text{Zn}_{1.9}\text{Ni}_{0.1}\text{SiO}_4$  (a),  $\text{Zn}_{1.5}\text{Ni}_{0.5}\text{SiO}_4$  (b),  $\text{ZnNiSiO}_4$  (c), and  $\text{Zn}_{0.4}\text{Ni}_{1.6}\text{SiO}_4$ ,  $\text{Ni}_2\text{SiO}_4$  compositions produced by the precipitation method and the modified approach to this method, respectively.

#### 4. Conclusions

A cost-effective environmentally friendly precipitation route using silica hydrogel derived from serpentine minerals has been first applied for introducing nickel ions into willemite structure. The detailed investigations have shown that the suggested method is only applicable for  $\text{Zn}_{2-x}\text{Ni}_x\text{SiO}_4$  compositions with  $0 < x \leq 1.0$  and depending on nickel concentration introduced into in  $\text{SiO}_2\text{--NaOH--ZnCl}_2\text{--NiCl}_2\text{--H}_2\text{O}$  system during the precipitation procedure, different percentages of willemite, liebenbergite and NiO phases are crystallized by the heat treatment of the precipitated intermediates from 900 up to 1200 °C thereby imparting different hues of blue and green tints to the final products. In the products obtained from  $\text{Zn}_{1.9}\text{Ni}_{0.1}\text{SiO}_4$  composition the prevalence of willemite phase representing nickel-doped willemite is responsible for deeper blue color the intensity of which increases on heating up to 1200 °C. With the gradual increasing of nickel content and temperature the share of NiO phase that is great at 900 °C starts reducing and this process is accompanied by the increasing of liebenbergite phase co-existing with willemite one. During these phase transformations the deep blue tint becomes lighter and then transforms into green color which then gradually starts changing into yellowish green hue distinguished by thermal stability on heating up to 1200 °C due to  $\text{Ni}_2\text{SiO}_4$  phase domination (over 70 %) for  $\text{ZnNiSiO}_4$  composition.

The applied method modification implying NaCl separation from the intermediates heated at 900 °C has allowed performing the interaction between the reagents in  $\text{Zn}_{2-x}\text{Ni}_x\text{SiO}_4$  systems where  $1.2 \leq x \leq 2.0$  and has revealed that in the products obtained by 1-h

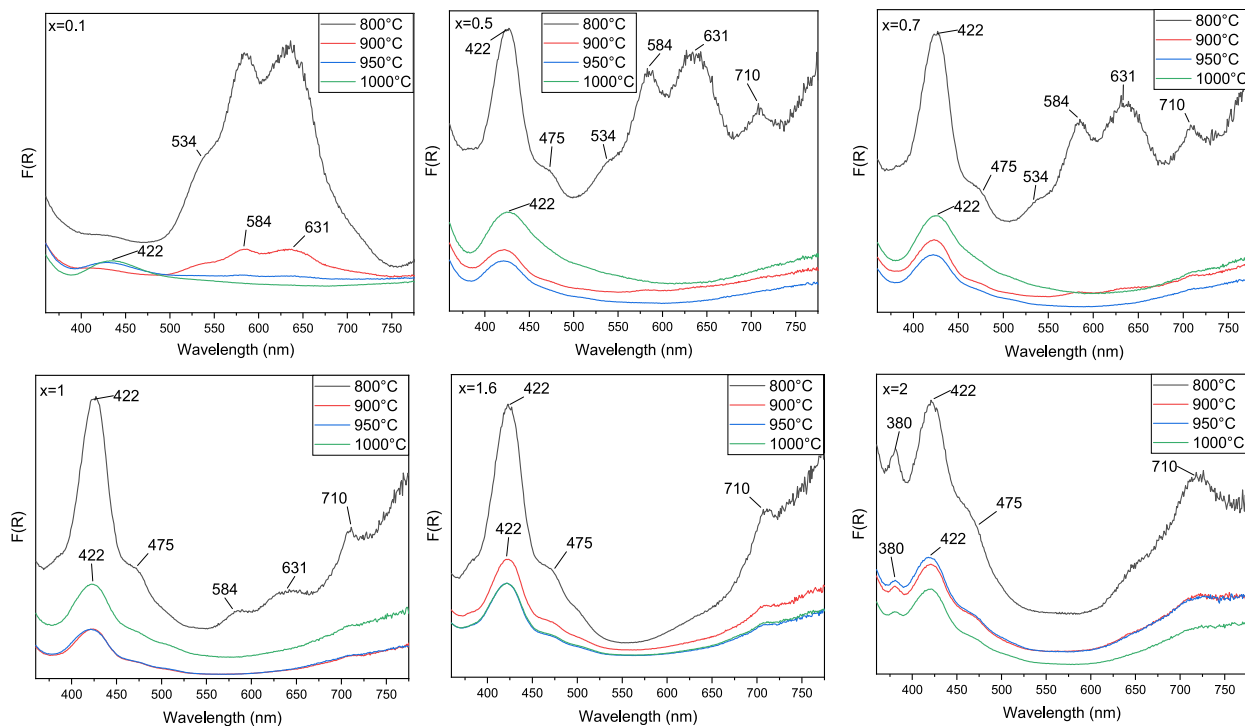


**Fig. 20.** SEM images and EDS mapping with element composition of the samples synthesized from  $Zn_{1.9}Ni_{0.1}SiO_4$  (a),  $Zn_{1.5}Ni_{0.5}SiO_4$  (b) and  $ZnNiSiO_4$  (c), and  $Zn_{0.4}Ni_{1.6}SiO_4$  (d) compositions by the precipitation method and the modified approach to this method, respectively.

**Table 3**

CIE-Lab parameters of the glazed wall tile samples containing 10 wt% of the pigments synthesized from the corresponding  $\text{Zn}_{2-x}\text{Ni}_x\text{SiO}_4$  compositions and heated at different temperatures.

x		800 °C	900 °C	950 °C	1000 °C
2.0	L*	60.05	72.34	72.32	79.71
	a*	-10.24	-9.60	-9.06	-8.49
	b*	22.89	20.19	21.07	23.59
1.6	L*	72.29	79.02	84.96	84.28
	a*	-16.65	-11.51	-11.52	-11.30
	b*	34.31	25.39	26.58	26.29
1.0	L*	64.57	87.10	86.95	75.10
	a*	-13.43	-8.07	-7.75	-5.82
	b*	19.82	19.12	19.14	16.98
0.7	L*	55.99	79.78	86.19	77.05
	a*	-14.31	-8.54	-5.37	-2.52
	b*	3.68	13.15	19.57	19.05
0.5	L*	56.93	81.45	86.73	76.66
	a*	-11.65	-5.05	-3.92	-1.18
	b*	0.01	9.59	14.09	14.47
0.1	L*	52.77	73.85	80.65	84.86
	a*	-3.32	-4.18	-2.57	0.29
	b*	-24.14	-8.64	7.048	14.83



**Fig. 21.** Absorbance spectra of the glazed wall tile samples containing 10 wt% of the pigments synthesized from the corresponding  $\text{Zn}_{2-x}\text{Ni}_x\text{SiO}_4$  compositions and heated at different temperatures. Ni-doped willemite-related bands: at 534, 584 and 631 nm;  $\text{Ni}_2\text{SiO}_4$ -related bands: at 422, 475 and 710 nm; NiO-related band: at 380 nm.

heat-treatment at 1200 °C from the compositions with x ranging from 1.2 up to 1.6 Ni<sub>2</sub>SiO<sub>4</sub> phase achieves 90 (±4) % thereby producing such a green pigment that yields olive green coloration stable in the glaze on heating up to 1000 °C. Hence, a novel low-temperature precipitation approach capable of producing the product largely composed of liebenbergite representing an excellent green pigment has been first developed. At the same time due to the decomposition of Ni-doped willemite the pigments largely composed of willemite phase impart the glaze light brown color.

### CRedit authorship contribution statement

**Hayk Beglaryan:** Visualization, Validation, Software, Resources, Project administration, Funding acquisition, Formal analysis, Data curation. **Anna Isahakyan:** Writing – review & editing, Writing – original draft, Data curation, Conceptualization. **Anna Terzyan:** Methodology, Investigation. **Vardanush Stepanyan:** Investigation. **Verzhine Sarkeziyan:** Investigation. **Nshan Zulumyan:** Supervision.

### Data and code availability statement

Data included in article is referenced in the article.

### Funding information

The work was supported by the Science Committee of RA, in the frames of the research projects № 21SCG-1D013 and № 21T-1D131.

### Declaration of competing interest

The authors declare the following financial interests/personal relationships which may be considered as potential competing interests: Beglaryan Hayk reports financial support was provided by The RA Ministry of Education, Science, Culture and Sports Higher Education and Science Committee. If there are other authors, they declare that they have no known competing financial interests or personal relationships that could have appeared to influence the work reported in this paper.

### References

- [1] T. Dimitrov, I. Markovska, T. Ibrev, The analysis about synthesis, structure and properties of willemite ceramic pigments obtained by a sol–gel method, *IOP Conf. Ser. Mater. Sci. Eng.* 893 (2020) 012001.
- [2] I. Ivanova, N. Zaitseva, R. Samigullina, I. Baklanova, M. Rotermel, Synthesis and crystal-chemical, thermal, and spectrochemical properties of the Zn<sub>2</sub>–2xNi<sub>2</sub>xSiO<sub>4</sub> solid solution with a willemite structure, *Russ. J. Inorg. Chem.* 65 (2020) 1535–1540.
- [3] A. Martin, L. Schabbach, M. Folgueras, Synthesis of nickel pigments using waste foundry sand as a silica source, *Cerámica*. 65 (2019) 562–568.
- [4] T. Ibrev, T. Dimitrov, I. Markovska, Synthesis and Study of Ni-Doped Willemite Ceramic Pigments, 2019, pp. 173–178.
- [5] I. Markovska, T. Dimitrov, T. Ibrev, Synthesis and characterization of willemite ceramic pigments suitable for the ceramic industry by utilization of Rice Husk Ash, *J. Chem. Biol. Phys. Sci.* 9 (4) (2019) 219–232.
- [6] L.A. Vieira, M.V. Folgueras, M. Tomiyama, S.R. Prim, Rice husk ash as a raw material to produce willemite pigments, *Mater. Sci. Forum* 912 (2018) 44–49.
- [7] W.-C. Tsai, K.-C. Chiu, Y.-X. Nian, Y.-C. Liou, Significant improvement of the microwave dielectric loss of Zn<sub>1.95</sub>M<sub>0.05</sub>SiO<sub>4</sub> ceramics (M = Zn, Mg, Ni, and Co) prepared by reaction-sintering process, *J. Mater. Sci. Mater. Electron.* 28 (19) (2017) 14258–14263.
- [8] B.C. Babu, S. Buddhudu, Synthesis and characterization of Ni<sub>2</sub>+: Zn<sub>2</sub>SiO<sub>4</sub> nano phosphor by sol-gel method, *AIP Conf. Proc.* 1447 (1) (2012) 1325–1326.
- [9] B. Chandra Babu, S. Buddhudu, Analysis of structural and electrical properties of Ni<sub>2</sub>+:Zn<sub>2</sub>SiO<sub>4</sub> ceramic powders by sol–gel method, *J. Sol. Gel Sci. Technol.* 70 (3) (2014) 405–415.
- [10] R.M. Krsmanović, Ž. Antić, M. Mitrić, M.D. Dramićanin, M.G. Brik, Structural, spectroscopic and crystal field analyses of Ni<sup>2+</sup> and Co<sup>2+</sup> doped Zn<sub>2</sub>SiO<sub>4</sub> powders, *Appl Phys A* 104 (1) (2011) 483–492.
- [11] C.-Y. Lee, H.-S. Lee, B.-H. Lee, A study on the NiO-doped willemite pigments, *J. Korean Ceram. Soc.* 48 (2011) 134–140.
- [12] S.R. Lukić, D. Petrović, L. Daćanin Far, M. Marinović-Cincović, Ž. Antić, R. Krsmanović Whiffen, et al., Gel combustion synthesis of transition metal ions doped Zn<sub>2</sub>SiO<sub>4</sub> powder, *J. Optoelectron. Adv. Mater.* 10 (2008) 2748.
- [13] G.T. Chandrappa, S. Ghosh, K.C. Patil, Synthesis and properties of willemite, Zn<sub>2</sub>SiO<sub>4</sub>, and M<sup>2+</sup>:Zn<sub>2</sub>SiO<sub>4</sub> (M = Co and Ni), *J. Mater. Synth. Process.* 7 (5) (1999) 273–279.
- [14] CPMA, Classification and Chemical Description of the Complex Inorganic Color Pigments, Alexandria, Dry Color Manufacturers Association, 2010.
- [15] M. Hosseini, M. Ghanbari, E.A. Dawi, M.A. Mahdi, S.H. Ganduh, L.S. Jasim, et al., Investigations of nickel silicate for degradation of water-soluble organic pollutants, *Int. J. Hydrogen Energy* 61 (2024) 307–315.
- [16] M. El Hadri, N. Siragi, H. Ahamdane, M.A. El Idrissi Raghni, Liebenbergite (Ni<sub>2</sub>SiO<sub>4</sub>): sol gel synthesis and comparative study of its color properties and those of the related Ni-doped forsterite green pigments, *J. Eur. Ceram. Soc.* 39 (16) (2019) 5442–5456.
- [17] S. Bayat, A. Sobhani, M. Salavati-Niasari, Simple sol–gel green auto combustion synthesis by using carbohydrate sugars as a novel reducing agent, characterization, photocatalytic behavior and slow-burning property of Ni<sub>2</sub>SiO<sub>4</sub> nanocomposites, *J. Mater. Sci. Mater. Electron.* 28 (22) (2017) 16981–16991.
- [18] D. Esteves, W. Hajjaji, M.P. Seabra, J.A. Labrincha, Use of industrial wastes in the formulation of olivine green pigments, *J. Eur. Ceram. Soc.* 30 (15) (2010) 3079–3085.
- [19] R. Vallepu, A. Mikuni, R. Komatsu, K. Ikeda, Synthesis of liebenbergite nano-crystallites from silicate precursor gels prepared by geopolymerization, *J. Mineral. Petrol. Sci.* 100 (4) (2005) 159–167.
- [20] N.O. Zulumyan, A.R. Isaakyan, Z.G. Oganessian, A new promising method for processing of serpentinites, *Russ. J. Appl. Chem.* 80 (6) (2007) 1020–1022.
- [21] H. Beglaryan, A. Isahakyan, A. Terzyan, V. Stepanyan, D. Elovikov, V. Gusarov, et al., Precipitation synthesis of Zn<sub>2</sub>-xCoxSiO<sub>4</sub> blue ceramic pigments: color performance and application, *Ceram. Int.* 50 (12) (2024) 21386–21395.
- [22] N.O. Zulumyan, A.R. Isaakyan, P.A. Pirumyan, A.A. Beglaryan, The structural characteristics of amorphous silicas, *Russ. J. Phys. Chem. A* 84 (4) (2010) 700–702.
- [23] A.R. Isahakyan, H.A. Beglaryan, P.A. Pirumyan, L.R. Papakhchyan, N.H. Zulumyan, An IR spectroscopic study of amorphous silicas, *Russ. J. Phys. Chem. A* 85 (1) (2011) 72–75.

- [24] H. Beglaryan, A. Isahakyan, N. Zulumyan, S. Melikyan, A. Terzyan, A study of magnesium dissolution from serpentinites composed of different serpentine group minerals, *Miner. Eng.* 201 (2023) 108171.
- [25] H.A. Beglaryan, S.A. Melikyan, N.H. Zulumyan, A.M. Terzyan, A.R. Isahakyan, Influence of colloid synthesis techniques on barium silicates formation using silica hydrogel derived from serpentine minerals, *J. Mol. Liq.* 291 (2019) 111263.
- [26] H. Beglaryan, A. Isahakyan, N. Zulumyan, S. Melikyan, A. Terzyan, A study of zinc silicate phases produced via a simplified method, *J. Therm. Anal. Calorim.* 148 (9) (2023) 3249–3262.
- [27] Y. Liang, C.R. Miranda, S. Scandolo, Infrared and Raman spectra of silica polymorphs from an ab initio parametrized polarizable force field, *J. Chem. Phys.* 125 (19) (2006) 194524.
- [28] C. Koike, R. Noguchi, H. Chihara, H. Suto, O. Ohtaka, Y. Imai, et al., Infrared spectra of silica polymorphs and the conditions of their formation, *Astrophys. J.* 778 (1) (2013) 60.
- [29] P.V. Kamath, S. Ganguly, Infrared spectroscopic studies of the oxide-hydroxides of Ni, Co and Mn, *Mater. Lett.* 10 (11) (1991) 537–539.
- [30] V. Biju, M. Abdul Khadar, Fourier transform infrared spectroscopy study of nanostructured nickel oxide, *Spectrochim. Acta Mol. Biomol. Spectrosc.* 59 (1) (2003) 121–134.
- [31] M. Venkatachalapathy, K. Sambathkumarb, N.R. Kamal, Synthesis and characterization of structural and magnetic properties of Fe doped NiO nanoparticles, *Dig. J. Nanomater. Biostruct.* 19 (1) (2024) 451–458.
- [32] S. Sagadevan, J. Podder, Investigations on structural, optical, morphological and electrical properties of nickel oxide nanoparticles, *Int. J. Nanoparticles (IJNP)* 8 (3–4) (2015) 289–301.
- [33] P.K. Sharma, M.K. Singh, G.D. Sharma, A. Agrawal, NiO nanoparticles: facile route synthesis, characterization and potential towards third generation solar cell, *Mater. Today: Proc.* 43 (2021) 3061–3065.
- [34] A.E. Lavat, G.X. Gayo, In situ formation of coloured M(II)-doped Zn<sub>2</sub>SiO<sub>4</sub>-willemite in ceramic glazes (M=Mn, Co, Ni, Cu), *Ceram. Int.* 40 (8, Part A) (2014) 11947–11955.